SUPPORTING INFORMATION

Charge transfer characteristics of fullerene-free polymer solar cells via multi-state electronic coupling treatment

Tuuva Kastinen[†,*] and Terttu I. Hukka[†,*]

[†] *Chemistry and Advanced Materials, Faculty of Engineering and Natural Sciences, Tampere University, P.O. Box 541, FI-33014 Tampere University, Finland. E-mail: tuuva.kastinen@tuni.fi, terttu.hukka@tuni.fi.*

Contents

Models: eD–eA complexes

Several configurations of the eD–eA complexes were constructed by superposing different backbone units of the eD and eA compounds. In all cases, the initial intermolecular distance, which was measured between the centres of mass of these backbone units, was set at 4.0 Å. After this, the geometries of the complexes were fully optimized (see Methods in the main article). Although, several configurations were considered, only the most representative ones, e.g. the most stable ones, were selected for further characterization. In each complex system, these included the configurations, where the acceptor (A) unit of the eA compound was either on the top of the donor (D) unit (i.e. the DA configurations) or acceptor unit (i.e. the AA configurations) of the eD compound. For BDT-TzBI–NDI2OD-T2 we considered also the configuration, where the acceptor unit of NDI2OD-T2 was on the top of the thiophene (the one between the donor and acceptor units, i.e. the TA(1) model). This first series of the BDT-TzBI–NDI2OD-T2 complexes, where the donor and acceptor units of both BDT-TzBI and NDI2OD-T2 were on the same direction, i.e. in the order of D–A, is marked with additional (1). For comparison, we had also one configuration, where the donor and acceptor units of BDT-TzBI and NDI2OD-T2 were on the different directions, which will be marked with DA(2). For comparison, the DA(2) configuration was constructed also from the dimer models of PBDT-TzBI and P(NDI2OD-T2). The optimized ground-state (GS) geometries of different complex configurations of the studied PSC systems are presented in Tables S8–S10.

Methods: additional details

Tuning of the range-separation parameters. For the individual compounds, the range-separation parameter (ω) in ωB97X-D was optimally tuned (OT) in vacuum with the gap tuning procedure[1,2] by minimizing the following equation:

$$J_{gap}(\omega)^2 = \sum_{i=0}^{1} \left[\varepsilon_{HOMO}^{\omega}(N+i) + IE^{\omega}(N+i) \right]^2,$$

(S1)

where $\varepsilon^{\omega}_{HOMO}(N+i)$ and $IE^{\omega}(N+i)$ are the HOMO energy and the vertical ionization energy (VIE) of the $(N+i)$ electron system, respectively, the N electronic system corresponding to the neutral compound and the $(N+1)$ electronic system to the anion. For the eD–eA complexes, the gap tuning procedure[2–5], which take both the IE of the eD compound and the electron affinity (EA) of the eA compound into account, was used:

$$J(\omega) = \left| \varepsilon_{HOMO,eD}^{\omega}(N) + E_{eD}^{\omega}(N-1) - E_{eD}^{\omega}(N) \right| + \left| \varepsilon_{HOMO,eA}^{\omega}(M+1) + E_{eA}^{\omega}(M) - E_{eA}^{\omega}(M+1) \right|,$$ (S2)

where $\varepsilon^{\omega}_{HOMO,eD}(N)$ and $\varepsilon^{\omega}_{HOMO,eA}(M+1)$ are the HOMO energies for the neutral eD and the anion of eA, respectively, $E^{\omega}_{eD}(N)$ and $E^{\omega}_{eA}(M)$ are the total energies of the neutral eD and eA, respectively, and $E^{\omega}_{eD}(N-1)$ and $E^{\omega}_{eA}(M+1)$ are the total energies of the cation of eD and the anion of eA, respectively. Here we assume that the eD and eA molecules dominate the IE and EA,

respectively. For each ω in the studied range, the VIE was always calculated as the energy difference between the cation and the neutral compound, which were at the optimized neutral geometry. Similarly, the vertical EA (VEA) was calculated as the energy difference between the neutral and the anion, both at the optimized anion geometry.

Bond length alternations. Bond length alternations (BLA) were calculated for the optimized GS geometries of the neutral, cationic, and anionic states and optimized geometries of the lowest excited singlet state (S_1) of BDT-TzBI, DTB-EF-T, and BDB-T-2F ($n = 3$ for all three) and NDI2OD-2T ($n = 4$). Each BLA value was calculated as the average difference in between the adjacent C–C single and C=C double bonds along the conjugation path in the molecule (Figure 5 in the main article), i.e. within the shortest path between the terminal carbon atoms in the backbone. Due to the chain end effects present in the finite oligomeric models, we considered BLAs for the innermost CRUs (BLA_{middle}) alongside with the total BLA values (BLA_{total}), as BLAs taken from the middle units correspond better to those of the periodic model of a copolymer[6].

Ionization energies and electron affinities. Both vertical and adiabatic IEs and EAs of the studied eD and eA compounds were calculated[7]. The VIE was calculated as the difference between the total energies of the cation (+) and the corresponding neutral system (0), which were both at the optimized (ground state) geometry of the neutral system:

$$VIE = E^+(0) - E^0(0) \qquad\qquad (S3)$$

Similarly, the VEA was calculated as the difference between the total energies of the neutral system and corresponding anion (−), which were both at the optimized (GS) geometry of the neutral system:

$$VEA = E^0(0) - E^-(0) \qquad\qquad (S4)$$

Adiabatic IE (AIE) was calculated as the difference between the total energies of the cation and the corresponding neutral system at their optimized (GS) geometries:

$$AIE = E^+(+) - E^0(0) \qquad\qquad (S5)$$

Adiabatic EA (AEA) was calculated as the difference between the total energies of a neutral system and the corresponding anion at their optimized (GS) geometries:

$$AEA = E^0(0) - E^-(-) \qquad\qquad (S6)$$

In the eq. S3–S6, the superscript refers to the electronic state and the value in the parentheses to the optimized geometry.

Reorganization energies. Intramolecular reorganization energies for the hole (λ_h) and electron (λ_e) transfer of the individual eD and eA compounds were calculated with the following equations[8,9]:

$$\lambda_h = [E^0(+) - E^0(0)] + [E^+(0) - E^+(+)] \tag{S7}$$

$$\lambda_e = [E^0(-) - E^0(0)] + [E^-(0) - E^-(-)] \tag{S8}$$

For the eD–eA complexes of the NF PSC systems with monomer models for copolymers, the reorganization energies of the ED and CR processes were considered to compose of the inner (λ_i) and outer (λ_s) contributions,

$$\lambda = \lambda_i + \lambda_s. \tag{S9}$$

The inner part of the reorganization energy is caused by the changes in the eD and eA equilibrium geometries upon CT and can be determined as the difference between the energy of the reactants (or products) in the geometry of the products (or reactants) and that of their equilibrium geometry. As the parabolas of the reactants and products do not always have the same shapes, they will lead to different values of λ_i, for which reason λ_i is usually estimated as the average value of the reorganization energies in the reactant and product states.[10] Thus, we have calculated λ_i for the ED processes of the local interfacial eD–eA complexes as follows[10,11]:

$$\lambda_{i,ED} = (\lambda_{i1,ED} + \lambda_{i2,ED})/2 \tag{S10}$$

$$\lambda_{i1,ED} = \left[E^{eD^*}(eD^+) + E^{eA}(eA^-) \right] - \left[E^{eD^*}(eD^*) + E^{eA}(eA) \right] \tag{S11}$$

$$\lambda_{i2,ED} = \left[E^{eD^+}(eD^*) + E^{eA^-}(eA) \right] - \left[E^{eD^+}(eD^+) + E^{eA^-}(eA^-) \right] \tag{S12}$$

where eD^* and eD^+ are the S_1 and cationic states of the isolated eD compound, respectively, and eA and eA^- are the neutral and anionic states of the isolated eA compound, respectively. The superscripts refer to the electronic state and the terms in the parentheses refer to the optimized geometries at which the SP energies are calculated. Similarly, λ_i for the CR process have been calculated with the following equations[12]:

$$\lambda_{i,CR} = (\lambda_{i1,CR} + \lambda_{i2,CR})/2 \tag{S13}$$

$$\lambda_{i1,CR} = \left[E^{eD^+}(eD) + E^{eA^-}(eA) \right] - \left[E^{eD^+}(eD^+) + E^{eA^-}(eA^-) \right] \tag{S14}$$

$$\lambda_{i2,CR} = \left[E^{eD}(eD^+) + E^{eA}(eA^-) \right] - \left[E^{eD}(eD) + E^{eA}(eA) \right] \tag{S15}$$

where eD refers to the (neutral) GS of the isolated eD.

The outer part of the reorganization energy is due to the changes in the electronic and nuclear polarizations and relaxation of the surrounding medium upon CT.[10] The classical dielectric continuum model developed by Marcus[13] can be employed for calculating λ_s with an assumption that the CT occurs in an isotropic dielectric environment. However, the uncertainties in the calculated parameters entering this model make the accurate prediction of λ_s rather a difficult task[14]. Thus, like in the previous studies carried out by us[5] and others[15,16], we have chosen to keep it as an adjusted parameter and calculated the rate constants with λ_s of 0.1–0.75 eV.

Gibbs free energy. The Gibbs free energy ($\Delta G°$) is the difference between the total energies of the complexes in their final and initial states.[10] Here we have used the Weller's equation for calculating $\Delta G°$ from the energies of the individual eD and eA compounds, while taking the Coulombic attraction (ΔE_{coul}) between their charged states into account.[10,11] For ED, $\Delta G°$ was calculated as

$$\Delta G_{ED}^{\circ} = E^{eD^+} + E^{eA^-} - E^{eD^*} - E^{eA} + \Delta E_{Coul,ED} \tag{S16}$$

where E^{eD^+} and E^{eD^*} are the total energies for the optimized cation and S_1 geometries of the isolated eD compound, respectively, and E^{eA^-} and E^{eA} are the total energies of the optimized anion and neutral (GS) geometries of the isolated eA compound, respectively. The Coulomb energy for ED is

$$\Delta E_{Coul,ED} = \sum_{eD^+}\sum_{eA^-} \frac{q_{eD^+} q_{eA^-}}{4\pi\varepsilon_0\varepsilon_s r_{eD^+ eA^-}} - \sum_{eD^*}\sum_{eA} \frac{q_{eD^*} q_{eA}}{4\pi\varepsilon_0\varepsilon_s r_{eD^* eA}} \tag{S17}$$

where q and r are the atomic charges and the distance between the charges, respectively, for the system defined by the subscript. The terms ε_0 and ε_s are the vacuum permittivity and the relative permittivity of the medium (i.e. static dielectric constant), respectively. The sums run over all atoms in each compound. The $\Delta G°$ value for the CR process is calculated in the similar way:

$$\Delta G_{CR}^{\circ} = E^{eD} + E^{eA} - E^{eD^+} - E^{eA^-} + \Delta E_{Coul,CR} \tag{S18}$$

where the Coulomb energy is

$$\Delta E_{Coul,CR} = \sum_{eD}\sum_{eA} \frac{q_{eD} q_{eA}}{4\pi\varepsilon_0\varepsilon_s r_{eDeA}} - \sum_{eD^+}\sum_{eA^-} \frac{q_{eD^+} q_{eA^-}}{4\pi\varepsilon_0\varepsilon_s r_{eD^+ eA^-}} \tag{S19}$$

The partial atomic charges, i.e. q in eq. S17 and S19 were calculated using the Merz–Singh–Kollman (MK) scheme[17,18].

Electronic coupling. Electronic couplings for the ED and CR processes of the studied eD–eA complexes were calculated with the multi-state version[19] of the FCD scheme[20], which we employed

in our previous study[5] of the complexes consisting of the copolymer TQ and fullerene derivative PC$_{71}$BM. In the FCD, a charge difference operator (Δq) is employed for transforming the adiabatic states to the diabatic ones, while assuming, that the transition densities (Δq_{if}) between the diabatic states localized at different sites (e.g. local and CT states) are zero. The system is partitioned into two fragments, which correspond to eD and eA. The elements in an adiabatic eD–eA charge difference matrix, $\mathbf{\Delta q^{ad}}$, are

$$\Delta q_{ij}{}^{ad} = \int\limits_{r \in eD} \rho_{ij}(r)\, dr - \int\limits_{r \in eA} \rho_{ij}(r)\, dr \tag{S20}$$

where $\rho_{ij}(\mathbf{r})$ is the one-particle density (if i = j) for the diagonal elements $\Delta q_{ii}{}^{ad}$ and $\Delta q_{jj}{}^{ad}$ defined as the eD–eA charge differences in the adiabatic states |i> and |j>, respectively, or the transition density for the off-diagonal terms $\Delta q_{ij}{}^{ad}$ (if i $\neq$ j). For the 2-state FCD[20], the coupling values can be obtained with the following formulation:

$$H_{if} = \frac{|\Delta q_{12}|\Delta E_{12}}{\sqrt{(\Delta q_1 - \Delta q_2)^2 + 4\Delta q_{12}{}^2}} \tag{S21}$$

In the multi-state FCD, the first step is to determine a unitary transformation matrix U1, which diagonalizes the adiabatic charge difference matrix ($\mathbf{\Delta q^{ad}}$):

$$U_1^T \Delta q^{ad} U_1 = U_1^T \begin{pmatrix} \Delta q_{11} & \Delta q_{12} & \Delta q_{13} & \cdots \\ \Delta q_{21} & \Delta q_{22} & \Delta q_{23} & \cdots \\ \Delta q_{31} & \Delta q_{32} & \Delta q_{33} & \cdots \\ \vdots & \vdots & \vdots & \ddots \end{pmatrix} U_1 = \begin{pmatrix} \Delta q_l & 0 & 0 & \cdots \\ 0 & \Delta q_m & 0 & \cdots \\ 0 & 0 & \Delta q_n & \cdots \\ \vdots & \vdots & \vdots & \ddots \end{pmatrix} \tag{S22}$$

Next, the same transformation is applied to the corresponding adiabatic Hamiltonian, i.e. the diagonal matrix $\mathbf{E}$ of the adiabatic energy, to obtain the Hamiltonian ($\mathbf{H}$):

$$U_1^T E U_1 = U_1^T \begin{pmatrix} E_1 & 0 & 0 & \cdots \\ 0 & E_2 & 0 & \cdots \\ 0 & 0 & E_3 & \cdots \\ \vdots & \vdots & \vdots & \ddots \end{pmatrix} U_1 = \begin{pmatrix} H_{ll} & H_{lm} & H_{ln} & \cdots \\ H_{ml} & H_{mm} & H_{mn} & \cdots \\ H_{nl} & H_{nm} & H_{nn} & \cdots \\ \vdots & \vdots & \vdots & \ddots \end{pmatrix} \tag{S23}$$

In the limiting case of the 2-state scheme, the diabatic charge difference matrix ($\mathbf{\Delta q^{diab}}$) and diabatic Hamiltonian ($\mathbf{H^{diab}}$) can be obtained already from eq. S22 and S23 (or alternatively from eq. S21), respectively. However, when multiple, i.e. more than two states are considered, there may exist several states that are localized on the same site, i.e. with the same nature. Therefore, $\mathbf{H}$ is re-diagonalized within the blocks of the same-site states to obtain the states, which are adiabatic within one block, but diabatic with respect to the states localized at different sites.[19] Thus, the states are first classified as the local states (LS, which includes GS, LE or LF states) or CT states according to their eigenvalues in the diagonalized $\mathbf{\Delta q}$ matrix (obtained from eq. S22). After this, $\mathbf{H}$ (obtained from eq. S23) is re-diagonalized within each block (i.e. CT1, LS, and CT2) to define the $\mathbf{H^{diab}}$:

$$U_2^T \begin{pmatrix} H_{LS} & H_{LS,CT} \\ H_{CT,LS} & H_{CT} \end{pmatrix} U_2 = \begin{pmatrix} E_{CT1} & \mathcal{H}_{CT1,LS} & \mathcal{H}_{CT1,CT2} \\ \mathcal{H}_{LS,CT1} & E_{LS} & \mathcal{H}_{LS,CT2} \\ \mathcal{H}_{CT2,CT1} & \mathcal{H}_{CT2,LS} & E_{CT2} \end{pmatrix} \tag{S24}$$

where a bold letter refers to a matrix in the LS, CT1, and CT2 subspaces defined by the subscript, $\mathbf{E}$ is a diagonal matrix, and the final electronic coupling values (H_{if}) are the corresponding off-diagonal matrix elements in $\mathcal{H}_{LS,CT}$. Finally, $\mathbf{\Delta q^{diab}}$ could be determined by applying the same transformation $\mathbf{U_2}$ to the diagonalized $\mathbf{\Delta q}$ obtained from eq. S22:

$$U_2^T \begin{pmatrix} \Delta q_l & 0 & 0 & \cdots \\ 0 & \Delta q_m & 0 & \cdots \\ 0 & 0 & \Delta q_n & \cdots \\ \vdots & \vdots & \vdots & \ddots \end{pmatrix} U_2 = \begin{pmatrix} \Delta q_{CT1}^{diab} & 0 & \Delta q_{CT1,CT2}^{diab} \\ 0 & \Delta q_{LS}^{diab} & 0 \\ \Delta q_{CT2,CT1}^{diab} & 0 & \Delta q_{CT2}^{diab} \end{pmatrix} \tag{S25}$$

Q-Chem uses the Mulliken population analysis for determining the atomic charges of the atoms in the FCD scheme. The Mulliken population analysis suffers from several problems, including the equally divided off-diagonal elements of the population matrix to two atoms regardless of their electronegativities. However, this problem is expected to have only a minor effect here, because the total charges on two fragments are calculated in FCD (see eq. S20).[21]

To keep the Gaussian and Q-Chem calculations consistent, the grid with 99 Euler–Maclaurin radial grid points and 302 Lebedev angular grid points, the SCF convergence criterion of 10^{-6}, and the cutoff for neglect of two electron integrals of 10^{-12} was employed in the Q-Chem coupling calculations. Moreover, the radii from the Universal Force Field (UFF) with a scaling factor of 1.1 was employed in conjunction with CPCM. Due to the SCF convergence problems of larger complexes, the iterative conjugate gradient (CG) solver was employed with the Precond, NoMatrix, and UseMultipole keywords.

Results: additional details

Optimally tuned range-separation parameters of OT-ωB97X-D

Table S1 *Optimally tuned (OT) range-separation parameters (ω) of OT-ωB97X-D for the isolated eD and eA compounds determined in vacuum using the gap tuning procedure[a] with the 6-31G** basis set.*

Type	Compound	OT ω (bohr^{-1})			
		$n = 1$	$n = 2$	$n = 3$	$n = 4$
eD	BDT-TzBI	0.12	0.09	0.09	-
	DTB-EF-T	0.11	-	0.09	-
	BDB-T-2F	0.11	-	0.10	-
eA	NDI2OD-2T	0.16	-	0.12	0.12
	ITIC	0.09			
	ITIC-4F	0.09			
	ITIC-2Cl	0.09			

[a]The OT ω values of the isolated molecules were determined using the gap tuning procedure described in ref. [1,2] see eq. S1.

Table S2 *Optimally tuned (OT) range separation parameters (ω) of OT-ωB97X-D for the eD–eA complexes determined in vacuum[a] with the 6-31G** basis set.*

Complex	OT ω (bohr^{-1})	
	Monomer models	**Dimer models**
BDT-TzBI–NDI2OD-T2	0.14	0.12
DTP-EF-T–ITIC-4F	0.10	-
BDB-T-2F–ITIC-2Cl	0.10	-

[a]The OT ω values of the complexes were determined from the OT ω values of the isolated eD and eA compounds using the gap tuning procedure described in ref. [2–5], eq. S2.

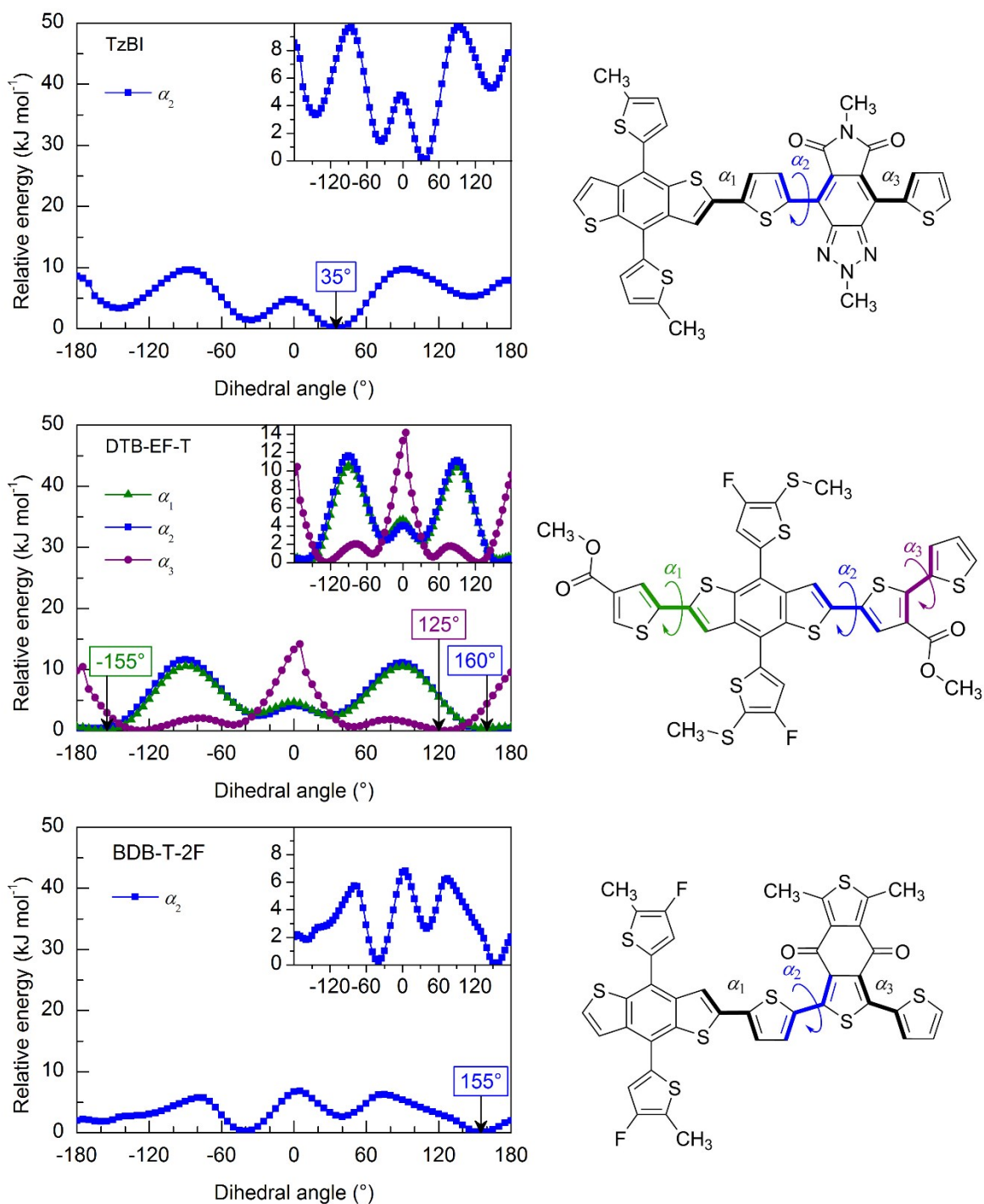# Conformational studies of the eD and eA compounds

Figure S1 *Relaxed PES curves for the scanned dihedral angles of the eD monomers calculated at the ωB97X-D/6-31G** level of theory in vacuum. The minimum (optimal) dihedral angles are presented in the graphs with the arrows.*
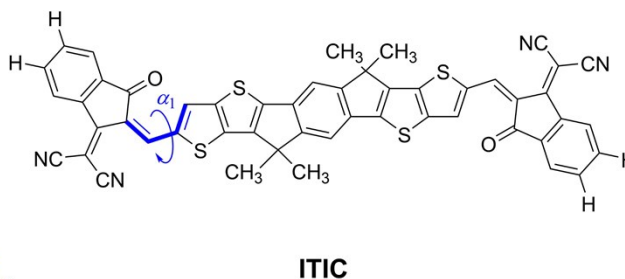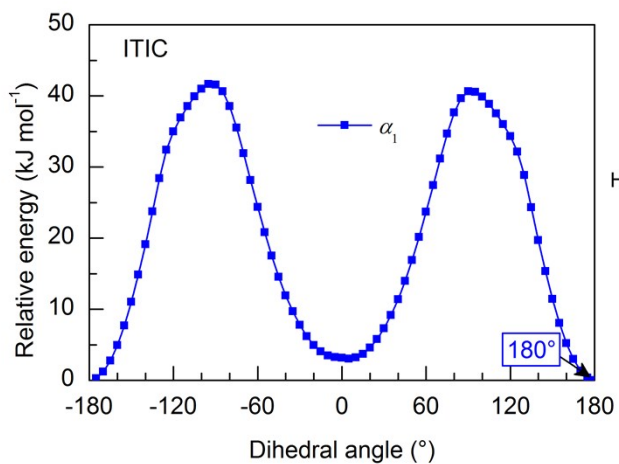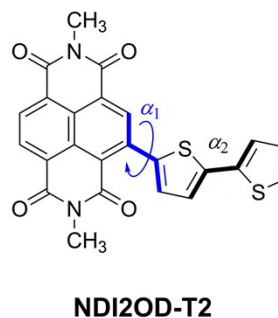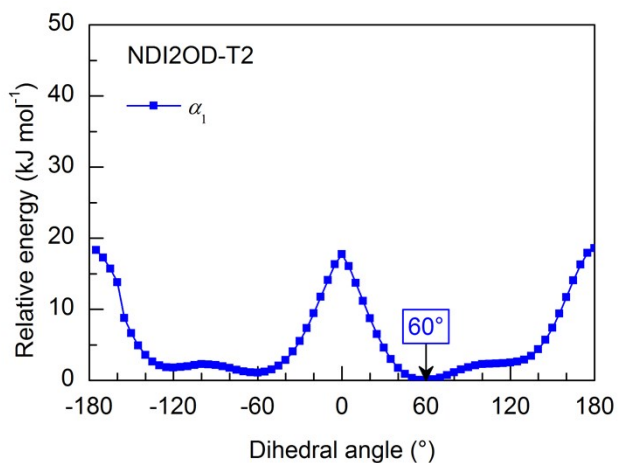
Figure S2 *Relaxed PES curves of the scanned dihedral angles of the monomer of the eA copolymer P(NDI2OD-T2) and the SMA ITIC calculated at the ωB97X-D/6-31G** level of theory in vacuum. The minimum (optimal) dihedral angles are also presented in the graphs.*
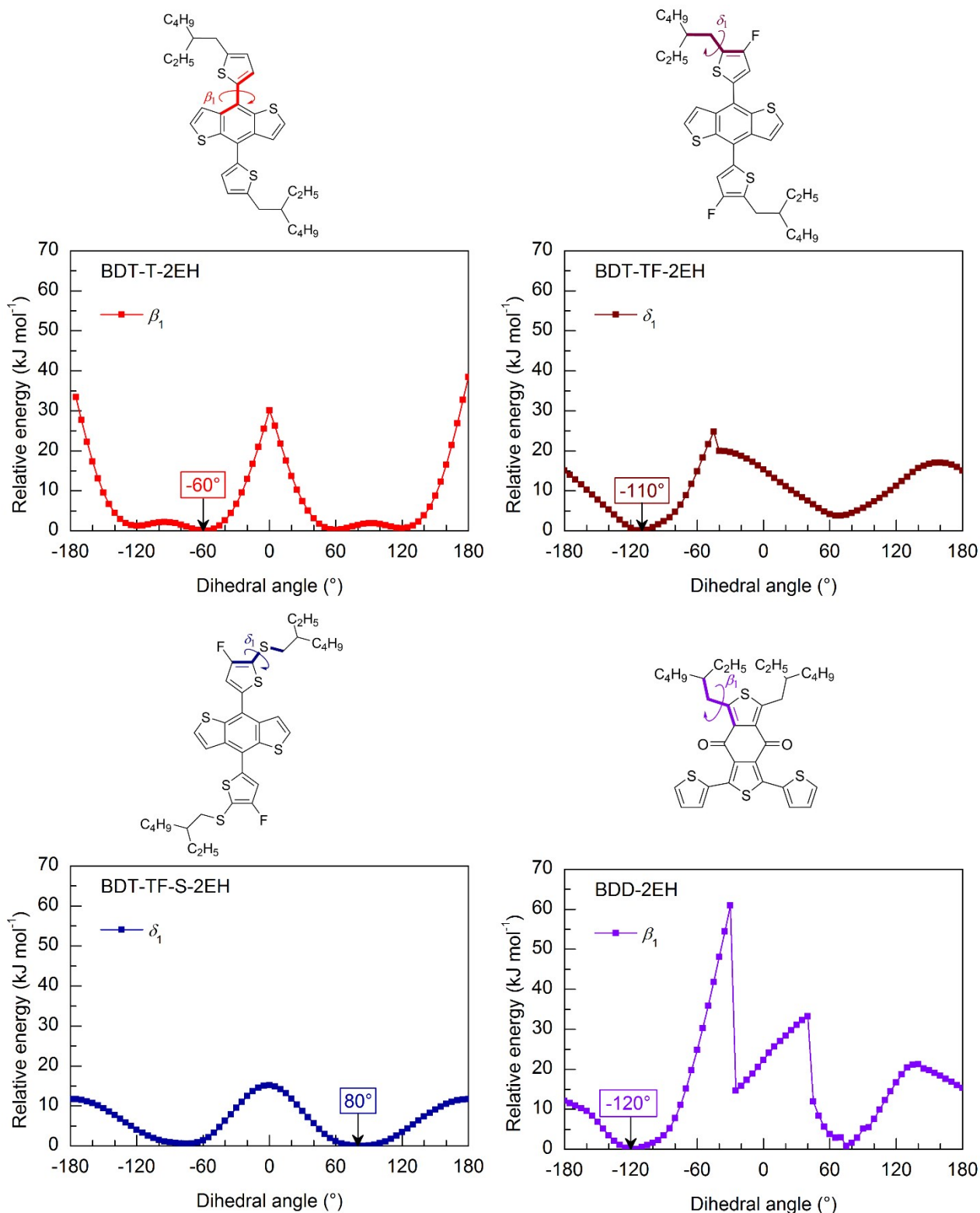
Relaxed PES scans of the side groups

Figure S3 *PES curves for the studied dihedral angles of the side groups in the BDT donor units of the eD models BDT-TzBI (BDT-T-2EH), BDB-T-2F (BDT-TF-2EH), and DTB-EF-T (BDT-TF-S-2EH) and in the BDD acceptor unit of BDB-T-2F (BDD-2EH) calculated at the ωB97X-D/6-31G** level of theory in vacuum. The minimum (optimal) dihedral angles are also presented in the graphs.*

Dihedral angles of the eD and eA compounds in vacuum and CHCl$_3$

Table S3 *Dihedral angles[a] (in degrees) for the optimized GS geometries of the studied eD and eA compounds calculated at the OT-ωB97X-D/6-31G** level of theory in two different environments.*

Type	Compound	n^b	Vacuum				CHCl$_3$			
			α_1	α_2	α_3	$\theta_{CRU–CRU}{}^c$	α_1	α_2	α_3	$\theta_{CRU–CRU}{}^c$
eD	BDT-TzBI	3	159	37	37–39	159	158–161	41–42	42–44	160–161
	DTB-EF-T	3	157–161	161–162	148–153	41	159-163	159-164	131-151	44–45
	BDB-T-2F	3	154–161	36–40	40–41	177	156–162	39–44	43–45	177
eA	NDI2OD-T2	4	54–56	150–151	-	58–60	56–58	152–154	-	60–61
	ITIC	-	0	-	-		0	-	-	
	ITIC-2Cl	-	0	-	-		0	-	-	
	ITIC-4F	-	0	-	-		0	-	-	

[a]See Figures S1–S2 for the definitions of the studied dihedral angles. [b]Number of the CRUs in the studied oligomer. [c]Between the CRUs in the oligomers.

Bond length alternations of the eD and eA compounds

Table S4 *BLA$_{total}$ values[a] of the studied eD and eA oligomers[b] calculated at the OT-ωB97X-D/6-31G** level of theory in vacuum, CHCl$_3$ (in parentheses), and blend (in brackets).*

Compound	BLA$_{total}$			
	S$_0$ (GS)	S$_1$	Cation	Anion
BDT-TzBI	0.049 (0.050) [0.050]	0.031 (0.031) [0.031]	0.035 (0.041) [0.041]	0.035 (0.040) [0.040]
DTB-EF-T	0.047 (0.049) [0.049]	0.029	0.032 (0.034) [0.035]	0.034 (0.038) [0.037]
BDB-T-2F	0.049 (0.050) [0.054]	0.031 (0.032) [0.032]	0.036 (0.039) [0.039]	0.040 (0.041) [0.041]
NDI2OD-T2	0.053 (0.054) [0.054]	-	0.040 (0.045) [0.044]	0.046 (0.051) [0.051]

[a]Calculated for the whole conjugation paths presented in Figure 5 in the main article. See "Bond length alternation" in "The methods: additional details" (above) for the calculation of the BLAs. [b]n = 3 for BDT-TzBI, DTB-EF-T, and BDB-T-2F and n = 4 for NDI2OD-2T.
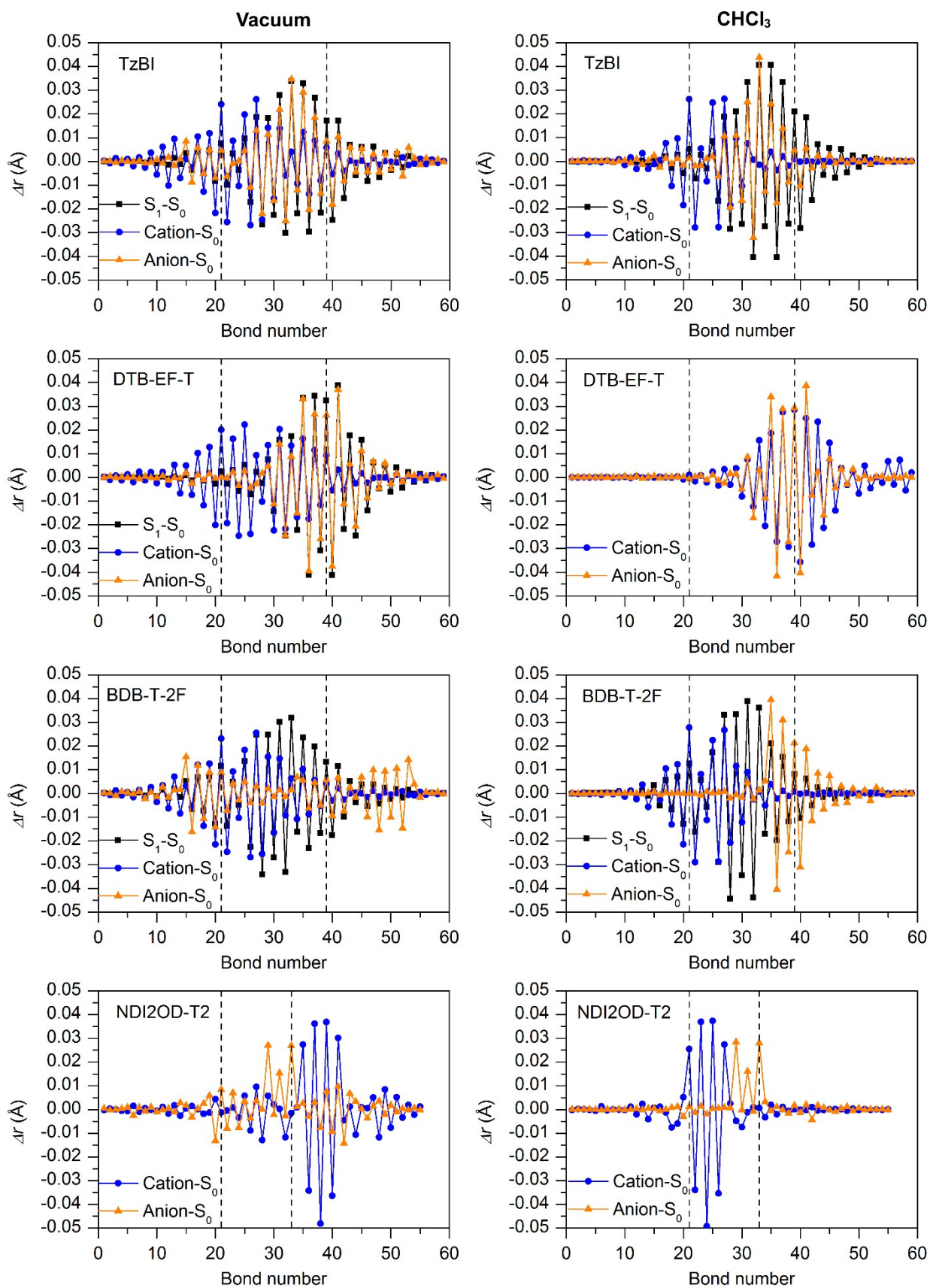
Figure S4 *Differences in bond lengths (Δr) between the OT-ωB97X-D/6-31**-optimized (in vacuum and CHCl₃) geometries of charged (cation, anion or S₁) and neutral (GS) compounds with respect to the bond numbers of the eD (n = 3) and eA (n = 4) oligomers along the conjugation paths presented in Figure 5 of the main article.*

Electronic properties of the eD and eA compounds

The calculated VIEs and AIEs (Figure S5 and Table S5) of the eD trimers increase in the order of BDT-TzBI < DTB-EF-T < BDB-T-2F in blend and $CHCl_3$ (in vacuum BDB-T-2F < DTB-EF-T) indicating that among them BDT-TzBI is the easiest to oxidize. The calculated VEAs and AEAs increase mostly in the order of BDB-T-2F < BDT-TzBI < DTB-EF-T (except for VEAs in $CHCl_3$ and blend) indicating that among the eD trimers BDB-T-2F is the easiest to reduce. For the eA compounds, the calculated VIEs and AIEs increase in the order of ITIC < ITIC-2Cl ≤ ITIC-4F < NDI2OD-T2. The VEAs of the eA compounds increase in the order of NDI2OD-T2 < ITIC < ITIC-2Cl < ITIC-4F. The ordering of AEAs is almost the same as for VEAs, i.e. ITIC < NDI2OD-T2 < ITIC-2Cl < ITIC-4F. This indicates that among the studied eA compounds, ITIC is the easiest to oxidize and reduce in most cases. The fluorinated and chlorinated derivatives of ITIC have larger IEs and EAs (both vertical and adiabatic) in all cases compared to ITIC, as can be expected based on the experimental values determined with the ultraviolet photoelectron spectroscopy (UPS)[22–26]. The calculated HOMO energies, which are also presented in Table S5 together with the HOMO–LUMO gaps, follow the same trends (BDT-TzBI < DTB-EF-T ≈ BDB < ITIC < ITIC-2Cl < ITIC-4F < NDI2OD-T2 in all media) as the negative VIEs, whereas the LUMO energies do not correlate as well with the VEA values. Overall, for the eA compounds the OT-ωB97X-D functional predicts VIEs quite close to the experimental VIEs[22–28], which have been derived from the UPS measurements (Figure S5; Table S5), whereas the VIE of the eD BDB-T-2F is somewhat larger than the experimental value[24]. The calculated VEAs of the eD and eA compounds are smaller than the experimental VEAs, in all cases[22–28].
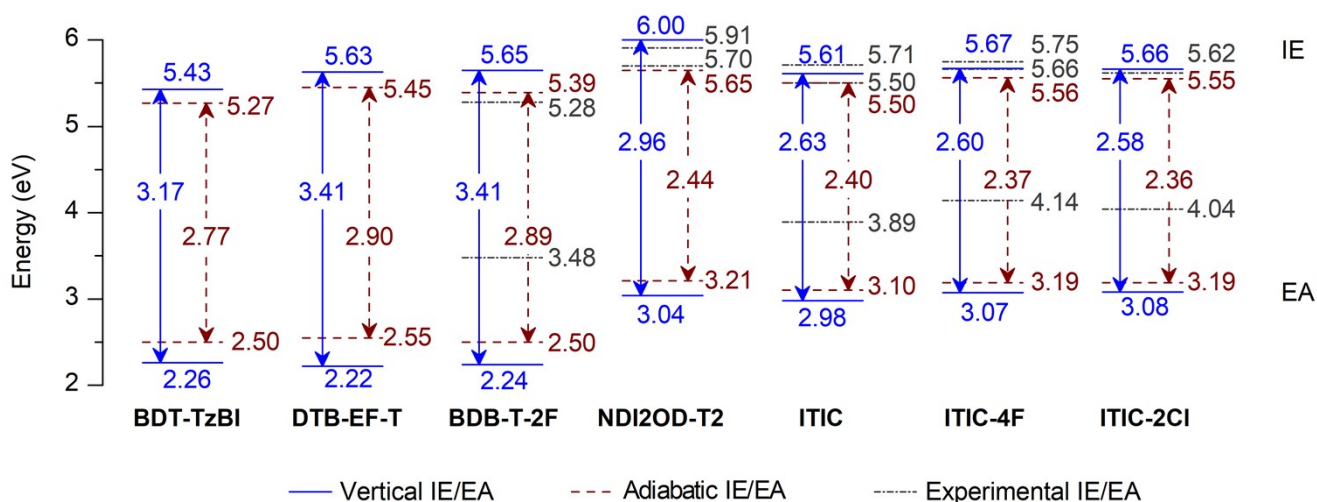

Figure S5 *Vertical and adiabatic IEs and EAs of the studied eD (the three leftmost) and eA (the four rightmost) compounds calculated at the OT-wB97X-D/6-31G** level of theory in blend; the reference values from the previous experimental UPS measurements. Arrows present the energy gaps between the IEs and EAs, the fundamental gap being the one between the vertical IE and EA.*

Table S5 *Electronic characteristics[a] (in eVs) of the studied eD and eA compounds[b] calculated in vacuum, CHCl$_3$ (in parentheses), and blend (in brackets) at the OT-ωB97X-D /6-31G** level of theory together with the corresponding experimental values[c].*

Compound	Method	HOMO	LUMO	E_{H-L}	VIE	VEA	AIE	AEA
BDT-TzBI	Calculated	-5.87 (-6.11) [-6.10]	-1.47 (-1.61) [-1.59]	4.40 (4.50) [4.51]	5.91 (5.40) [5.43]	1.43 (2.33) [2.26]	5.76 (5.24) [5.27]	1.65 (2.55) [2.50]
	Experimental	-5.34[29]	-3.46[29]	1.88[29]				
DTB-EF-T	Calculated	-6.13 (-6.24) [-6.23]	-1.55 (-1.60) [-1.59]	4.58 (4.64) [4.64]	6.17 (5.60) [5.63]	1.52 (2.26) [2.22]	6.03 (5.43) [5.45]	1.76 (2.60) [2.55]
	Experimental	-5.50[30]	-3.59[30]	1.93[30]				
BDB-T-2F	Calculated	-6.12 (-6.24) [-6.23]	-1.48 (-1.56) [-1.56]	4.64 (4.68) [4.67]	6.12 (5.61) [5.65]	1.37 (2.29) [2.24]	5.99 (5.37) [5.39]	1.46 (2.52) [2.50]
	Experimental	-5.54[31]; -5.42[32]	-3.65[31]; -3.36[32]	1.89[31]; 2.09[32]	5.28[24]	3.48[24]		
NDI2OD-T2	Calculated	-6.87 (-6.91) [-6.91]	-2.23 (-2.21) [-2.21]	4.64 (4.70) [4.70]	6.90 (5.95) [6.00]	2.20 (3.09) [3.04]	6.49 (5.60) [5.65]	2.42 (3.35) [3.21]
	Experimental	-5.81[33]	-3.84[33]	1.97[33]	5.70[27] 5.95[28]			
ITIC	Calculated	-6.34 (-6.35) [-6.35]	-2.33 (-2.38) [-2.37]	4.01 (3.97) [3.98]	6.32 (5.57) [5.61]	2.25 (3.02) [2.98]	6.20 (5.46) [5.50]	2.37 (3.13) [3.10]
	Experimental	-5.55[34]	-3.80[34]	1.75[34]	5.63[22]; 5.71[23]; 5.50[24]	3.89[24]		
ITIC-4F	Calculated	-6.48 (-6.40) [-6.40]	-2.50 (-2.46) [-2.46]	3.98 (3.94) [3.94]	6.45 (5.62) [5.67]	2.42 (3.10) [3.07]	6.33 (5.51) [5.56]	2.54 (3.22) [3.19]
	Experimental	-5.70[30]; -5.66[31]; -5.67[34];	-3.99[30]; -4.14[31]; -4.15[34]	1.71[30] 1.52[31,34]	5.66[24]; 5.75[23]; 5.68[25]	4.14[24,25]		
ITIC-2Cl	Calculated	-6.45 (-6.40) [-6.40]	-2.48 (-2.47) [-2.47]	3.97 (3.93) [3.93]	6.42 (5.62) [5.66]	2.41 (3.11) [3.08]	6.30 (5.51) [5.55]	2.53 (3.23) [3.19]
	Experimental	-5.68[34]	-3.99[34]	1.55[34]	5.62[26]	4.04[26]		

[a]HOMO, LUMO, and HOMO–LUMO gap energies (E_{H-L}). [b]In the case of the copolymers, $n = 3$ for BDT-TzBI, DTB-EF-T, and BDB-T-2F and $n = 4$ for NDI2OD-2T. [c]Experimental oxidation and reduction potentials measured with the cyclic voltammetry (CV) used for approximating the HOMO and LUMO energies, respectively. Experimental VIEs and VEAs as measured with UPS.

Excited-state characteristics of the eD and eA compounds

The wavelengths of the absorption maxima of the eD and eA compounds increase in the order of DTB-EF-T < BDB-T-2F < BDT-TzBI < NDI2OD-2T < ITIC < ITIC-4F < ITIC-2Cl in vacuum and CHCl$_3$ (Figure S6 and Table S6). In the blend environment, the order of BDB-T-2F and BDT-TzBI is reversed (i.e. BDT-TzBI < BDB-T-2F). The ordering of the calculated absorption maxima in blend corresponds to that of the experimental absorption maxima measured for the thin films. However, OT-ωB97X-D underestimates the wavelengths (i.e. overestimates the energies) with respect to the experimental values (see Table S6) indicating that the oligomers used here might not be long enough for correctly describing the spectra. Nevertheless, the shapes of the calculated UV-Vis spectra are consistent with the experimental ones showing a dual-band shape for the eD and eA oligomers which is typical for the D–A copolymers. Especially for NDI2OD-2T the dual absorption characteristics is clearly predicted. The calculations of the eD and eA compounds with the global hybrid PBE0 functional in CHCl$_3$ yield results somewhat closer to the experimental ones, although PBE0 underestimates the wavelengths, as well (Table S6).
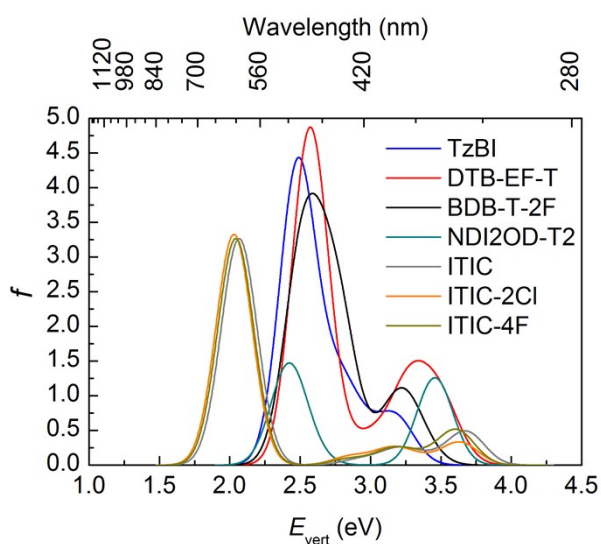

Figure S6 *UV-Vis absorption spectra of the eD and eA compounds calculated at the OT-ωB97X-D /6-31G** level of theory in CHCl$_3$.*

Table S6 *Optical properties[a] of the studied eD and eA compounds[b] calculated in vacuum, in CHCl$_3$ (in parentheses), and in blend (in brackets) at the OT-ωB97X-D /6-31G** level of theory, in CHCl$_3$ at the PBE0/6-31G** level of theory, and the experimental absorption maxima measured in solvent[c] and from thin film.*

	OT-ωB97X-D		PBE0		Experimental	
Compound	$E_{vert,max}$ **(eV/nm)**	f	$E_{vert,max}$ **(eV/nm)**	f	$E_{abs,max}$ **(eV/nm)**	**Ref.**
BDT-TzBI	2.43/511 (2.48/500) [2.49/498]	4.23 (4.21) [4.22]	(2.28/543)	(3.50)	2.27/545 (sol.) 2.04/608 (film)	35
DTB-EF-T	2.56/484 (2.57/483) [2.56/483]	4.67 (4.73) [4.70]	(2.40/517)	(4.23)	2.28/544 (sol.) 2.26/548 (film)	30
BDB-T-2F	2.49/497 (2.49/497) [2.49/498]	2.26 (2.29) [2.29]	(2.28/543)	(2.03)	2.25/552 & 2.10/591 (sol.) 2.00/621 (film)	32
NDI2OD-T2	2.38/522 (2.41/513) [2.27/547]	1.35 (1.34) [1.25]	(1.94/638)	(0.98)	1.85/672 (sol.) 1.78/696 (film)	36
ITIC	2.20/565 (2.07/600) [2.06/601]	2.93 (3.26) [3.28]	(1.90/651)	(2.95)	1.83/676 (sol.)[37] 1.78/698 (film)	34
ITIC-4F	2.17/571 (2.04/607) [2.04/609]	2.94 (3.26) [3.28]	(1.88/659)	(2.94)	1.73/718 (film)	34
ITIC-2Cl	2.16/573 (2.03/611) [2.03/612]	3.01 (3.33) [3.35]	(1.87/664)	(2.99)	1.72/720 (film)	34

[a]Vertical excitation energies ($E_{vert,max}$) and oscillator strengths (f) corresponding to the S$_0$→S$_1$ transition. [b]In the case of the copolymers, n = 3 for BDT-TzBI, DTB-EF-T, and BDB-T-2F and n = 4 for NDI2OD-2T. [c]Measured in CHCl$_3$, except for PDTB-EF-T ("P2" in the paper), which was measured in chlorobenzene.
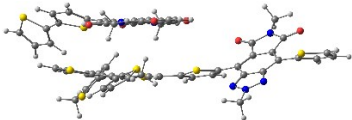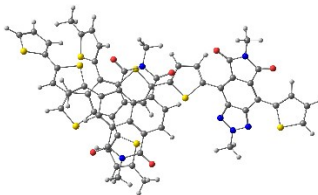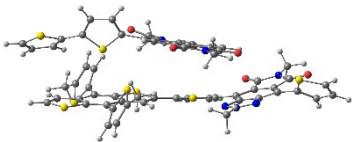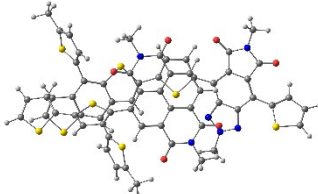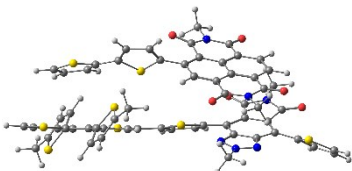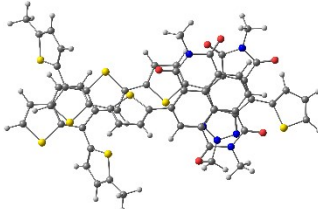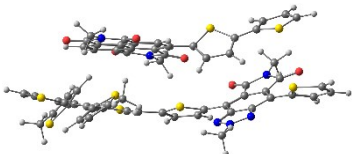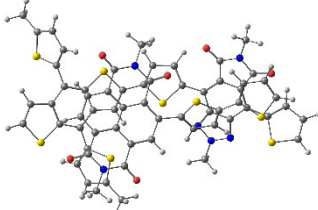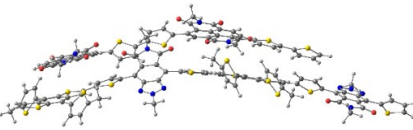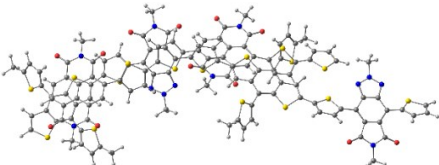
Table S7 *Contributions (%) of the electron densities of the donor (D), thiophene (T), and acceptor (A) backbone units to the NTOs[a] of the studied eD and eA compounds[b] calculated at OT-ωB97X-D /6-31G** level of theory in vacuum and CHCl₃ (in parentheses).*

Compound	λ_{NTO}	hole			electron		
		D	**T**	**A**	**D**	**T**	**A**
BDT-TzBI	0.6	42 (44)	40 (39)	18 (17)	24 (26)	28 (29)	48 (45)
DTB-EF-T	0.6	36 (37)	23 (22)	41 (41)	33 (32)	17 (18)	50 (50)
BDB-T-2F	0.6	40 (41)	39 (39)	21 (20)	30 (31)	33 (33)	37 (36)
NDI2OD-T2	0.6	78 (78)	-	22 (22)	13 (13)	-	87 (87)
ITIC	0.9	79 (79)	-	21 (21)	54 (54)	-	46 (46)
ITIC-4F	0.9	78 (78)	-	22 (22)	53 (53)	-	47 (47)
ITIC-2Cl	0.9	78 (78)	-	22 (22)	53 (53)	-	47 (47)

[a]For the $S_0 \rightarrow S_1$ transitions. The dominant pairs. [b]In the case of the copolymer models, $n = 3$ for BDT-TzBI, DTB-EF-T, and BDB-T-2F and $n = 4$ for NDI2OD-2T.

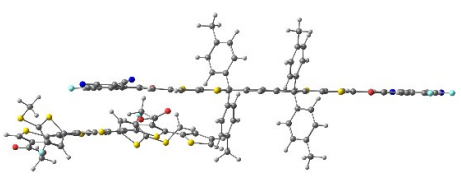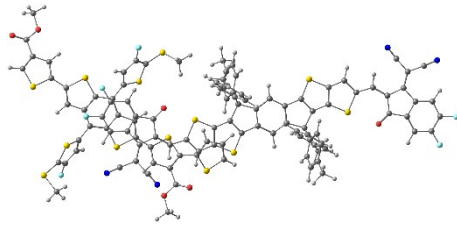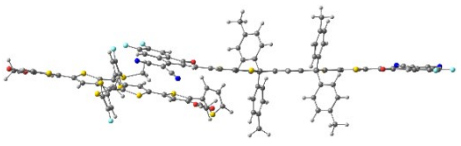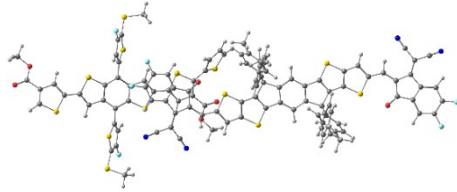**Optimized ground-state geometries of the eD–eA complexes**

Table S8 *Optimized GS geometries of the different configurations of the polymer–polymer system BDT-TzBI–NDI2OD-T2[a] and relative energies (ΔE_{rel})[b] calculated at the OT-ωB97X-D/6-31G** level of theory in blend.*

Configuration	ΔE_{rel} (kJ mol^{-1})	Side view	Top view
DA(1)	35.8		
TA(1)	16.0		
AA(1)	0.0		
DA(2)	0.9		
DA(2) dimers	-		

[a] In the (1) models, the donor and acceptor units of both BDT-TzBI and NDI2OD-T2 are on the same direction, whereas in the (2) model, the corresponding units of BDT-TzBI and NDI2OD-T2 are on the different directions (see "Models: eD–eA complexes" above). For both BDT-TzBI and NDI2OD-T2, $n = 1$ in the complex, except for the last configuration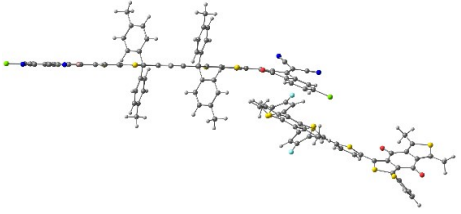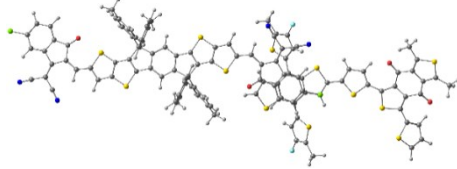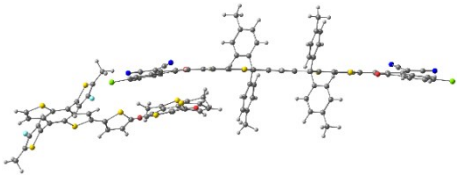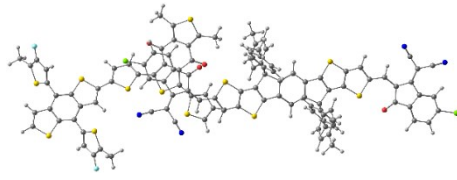 in the table, where $n = 2$ for both. [b]Calculated as the difference between the total energies of the particular configuration and the energetically most favourable configuration AA(1).

Table S9 *Optimized GS geometries of different configurations of the polymer–SMA system DTB-EF-T–ITIC-4F[a] and their relative energies (ΔE$_{rel}$) calculated at the OT-ωB97X-D/6-31G** level of theory in blend.*

Configuration	ΔE$_{rel}$ (kJ mol^{-1})	Side view	Top view
DA	0.0		
AA	17.2		
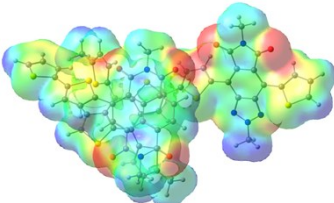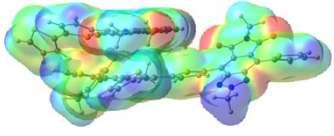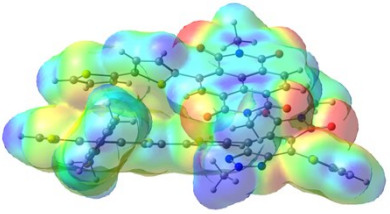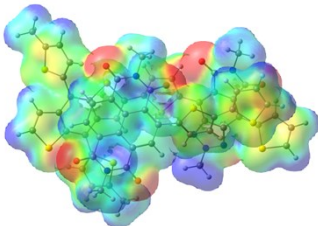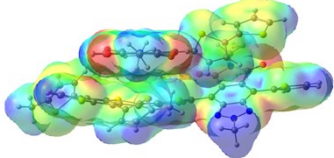
[a]For DTB-EF-T, *n* = 1. [b]Calculated as the difference between the total energy of the configuration in question and that of the energetically most favorable configuration.

Table S10 *Optimized GS geometries of different configurations of the polymer–SMA system BDB-T-2F–ITIC-2Cl[a] and their relative energies (ΔE$_{rel}$)[b] calculated at the OT-ωB97X-D/6-31G** level of theory in blend.*

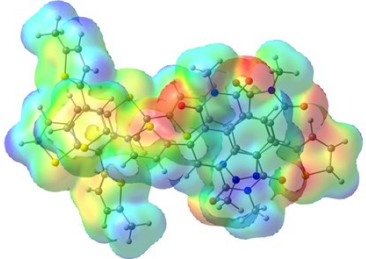| Configuration	ΔE$_{rel}$ (kJ mol^{-1})	Side view	Top view
DA	12.5		
AA	0.0		

[a]For BDB-T-2F, *n* = 1. [b]Calculated as the difference between the total energy of the configuration in question and that of the energetically most favorable configuration.

Table S11 *Electrostatic potential surfaces (EPS)[a] of the DA and AA configurations of the polymer–polymer system BDT-TzBI–NDI2OD-T2[b] calculated at the OT-ωB97X-D/6-31G** level of theory (in blend).*

Configuration	ΔE_{rel} (kJ mol^{-1})	EPS (top view)	EPS (side view)
DA(1)	35.8	-0.05 ▮ 0.05	-0.05 ▮ 0.05
AA(1)	0.0	-0.05 ▮ 0.05	-0.05 ▮ 0.05
DA(2)	0.9	-0.05 ▮ 0.05	-0.05 ▮ 0.05

[a]With the isodensity contour of 0.005. [b]For both BDT-TzBI and NDI2OD-T2, $n = 1$.

Intermolecular charge transfer: the AA(1) configuration of BDT-TzBI–NDI2OD-T2

Figure S7 *NTOs (the dominant pairs) for the CT and LE states of the BDT-TzBI–NDI2OD-T2 complex (the AA(1) configuration) calculated with TDDFT at the OT-ωB97X-D/6-31G** level of theory in blend.*

Electronic couplings with the 2- and multi-state treatments

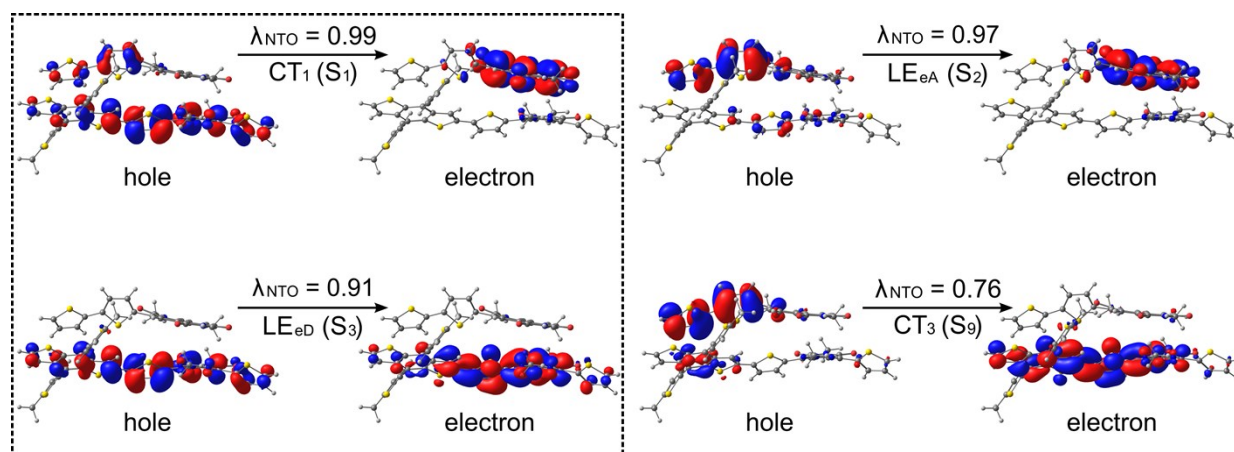The effect of the number of the states on the electronic couplings was examined for the BDT-TzBI–NDI2OD-T2 complex constructed from the single CRU models of the eD and eA copolymers (the AA(1) configuration, see Table S8). The electronic couplings were calculated with the multi-state FCD scheme (eq. S22–S24) using the vertical excitation energies and adiabatic charge differences (Δq_{ii} and Δq_{ij}) for the 10–25 lowest excited singlet states of BDT-TzBI–NDI2OD-T2. The 3–6 -state couplings were obtained in the corresponding manner as in our previous study of the copolymer–fullerene (TQ–PC$_{71}$BM) system[5], i.e. the adiabatic states (GS, CT$_1$, LE, CT$_2$, …) were selected from the output of a single, 11-state, calculation. In addition, separate calculations were done here for 16 and 26 states. In the case of BDT-TzBI–NDI2OD-T2, the multi-state calculations were mainly carried out by using the default solver, i.e. direct matrix inversion algorithm to solve the PCM equations in Q-Chem 4.2. However, due to the convergence problems of the slightly larger complexes, i.e. DTB-EF-T–ITIC-4F and BDB-T-2F–ITIC-2Cl, the conjugate gradient (CG) solver and additional keywords (see the methods above) were used for calculating the 11-state couplings and the corresponding CT rates presented in the main article. However, the solver algorithm does not seem to effect the 11-state electronic couplings (Table S12).

Table S12 *Electronic couplings for the ED and CR processes of the BDT-TzBI–NDI2OD-T2 complex[a] calculated with the FCD scheme at the OT-ωB97X-D/6-31G** level of theory (in blend) using different number of states.[b]*

Number of states[b]	Electronic coupling (meV)	
	ED	CR
2	19.67	51.02
3	19.70	51.37
4	19.84	51.16
5	19.38	51.10
6	18.92	51.03
11	16.55	47.76
11 (CG)[c]	16.55	47.76
11[d]	16.35	47.45
16	16.50	47.80
26	16.55	46.86

[a]The AA(1) configuration with the monomer models. [b]The 2-state FCD couplings were obtained directly from the output of the 11-state Q-Chem calculation; the multi-state (>2) values were determined using eq. S22–S24. The number of states is the amount of GS + excited singlet states. [c]With the CG solver, see the text above. [d]The states (11) were taken from the 26-state Q-Chem calculation.

Table S13 *Electronic couplings for the ED and CR processes of the polymer–SMA systems[a] calculated with the FCD scheme at the OT-ωB97X-D/6-31G** level of theory (in blend) using different number of states.[b]*

Complex	Configuration	Number of states[b]	Electronic coupling (meV)	
			ED	CR
DTB-EF-T–ITIC-4F	DA	2	102.24	107.17
		11	110.91	99.80
	AA	2	1.77	24.04
		11	0.35	24.38
BDB-T-2F–ITIC-2Cl	DA	2	7.60	69.89
		11	6.87	70.37
	AA	2	31.32	131.50
		11	33.82	131.83

[a] For copolymer models, $n = 1$. [b]The 2-state FCD couplings were obtained directly from the output of the 11-state Q-Chem calculation, the 11-state values were determined using eq. S22–S24.

Charge transfer parameters and rates

Table S14 *Contributions of the eD and eA compounds to the inner part of the reorganization energy[a] calculated at the OT-ωB97X-D/6-31G** level of theory (in blend) for the ED and CR processes of the eD–eA complexes[b].*

| | | Complex (eD–eA) configurations | | | | | | | |
| | | BDT-TzBI–NDI2OD-T2 | | | | DTB-EF-T–ITIC-4F | | BDB-T-2F–ITIC-2Cl | |
Process		DA(1)	TA(1)	AA(1)	DA(2)	DA	AA	DA	AA
$\lambda_{\text{i1,ED}}$	$E^{\text{eD}*}(\text{eD}^+) - E^{\text{eD}*}(\text{eD}^*)$	0.343	0.393	0.308	0.313	0.113	0.114	0.235	0.226
	$E^{\text{eA}}(\text{eA}^-) - E^{\text{eA}}(\text{eA})$	0.025	0.117	0.138	0.127	0.129	0.107	0.066	0.084
$\lambda_{\text{i2,ED}}$	$E^{\text{eD}+}(\text{eD}^*) - E^{\text{eD}+}(\text{eD}^+)$	0.203	0.202	0.201	0.201	0.063	0.064	0.131	0.128
	$E^{\text{eA}-}(\text{eA}) - E^{\text{eA}-}(\text{eA}^-)$	0.336	0.226	0.207	0.215	0.136	0.169	0.125	0.206
$\lambda_{\text{i1,CR}}$	$E^{\text{eD}+}(\text{eD}) - E^{\text{eD}+}(\text{eD}^+)$	0.190	0.243	0.206	0.181	0.201	0.208	0.157	0.186
$\lambda_{\text{i2,CR}}$	$E^{\text{eD}}(\text{eD}^+) - E^{\text{eD}}(\text{eD})$	0.010	0.083	0.098	0.070	0.125	0.158	0.132	0.118

[a]With eq. S10–S15. [b]For the copolymer models, *n* =1.

Table S15 *Coulomb energies (ΔE$_{Coul}$) for the ED and CR processes of the eD–eA complexes calculated[a] at the OT-ωB97X-D/6-31G** level of theory (in blend).*

Complex	Configuration	ΔE$_{\text{Coul,ED}}$ (eV)	ΔE$_{\text{Coul,CR}}$ (eV)
BDT-TzBI–NDI2OD-T2	DA(1)	-0.46	0.46
	AA(1)	-0.37	0.38
	TA(1)	-0.42	0.46
	DA(2)	-0.49	0.45
DTB-EF-T–ITIC-4F	DA	-0.33	0.31
	AA	-0.33	0.33
BDB-T-2F–ITIC-2Cl	DA	-0.20	0.18
	AA	-0.35	0.36

[a]With eq. S17 and S19.

Table S16 *Charge transfer rate parameters[a] for the ED and CR processes taking place at the local interfacial complexes calculated at the OT-ωB97X-D/6-31G** level of theory in blend.*

Complex	Configuration	$H_{\text{if,ED}}$ (meV)	$H_{\text{if,CR}}$ (meV)	$\lambda_{\text{in,ED}}$ (eV)	$\lambda_{\text{in,CR}}$ (eV)	$\Delta G°_{\text{ED}}$ (eV)	$\Delta G°_{\text{CR}}$ (eV)	k_{ED} (s^{-1})	k_{CR} (s^{-1})
BDT-TzBI–NDI2OD-T2	DA(1)	13.81	38.20	0.45	0.28	-0.85	-1.52	$2.74 \cdot 10^{12}$	$5.40 \cdot 10^{10}$
	TA(1)	46.77	105.03	0.44	0.33	-0.72	-1.70	$1.26 \cdot 10^{13}$	$7.19 \cdot 10^{10}$

[a]Electronic couplings (H_{if}) calculated with the multi-state (11 states) FCD scheme, inner reorganization energies (λ_{i}), Gibbs free energies ($\Delta G°$), and CT rates (k). External reorganization energy of 0.53 eV was used for calculating the CT rates.
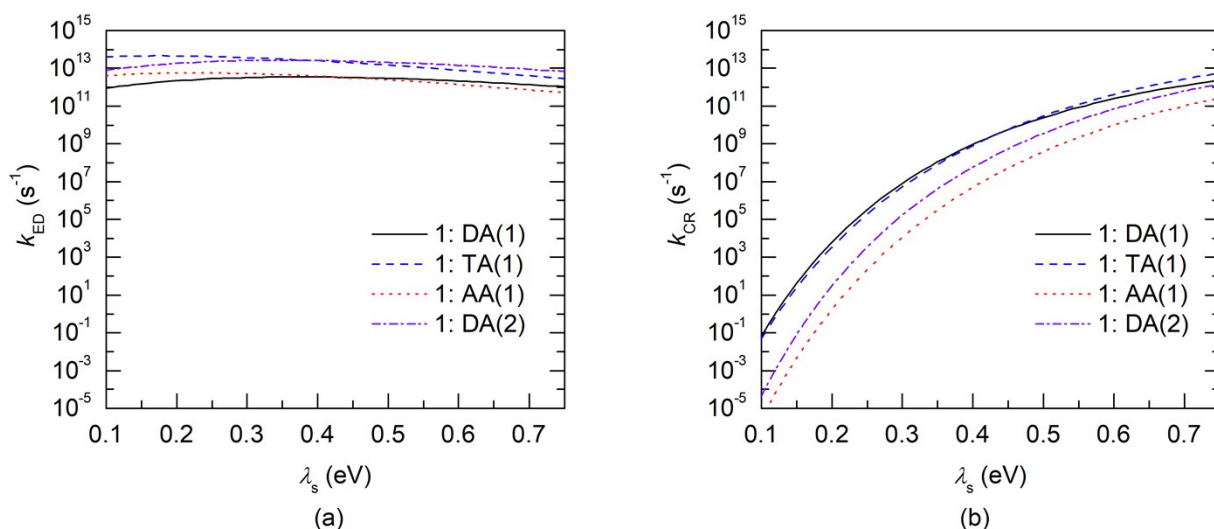
Figure S8 *Evolutions of the charge transfer rates (k_{ED} and k_{CR}) as functions of λ_s (0.1–0.75 eV) for the (a) ED and (b) CR processes of the BDT-TzBI–NDI2OD-T2 complexes calculated at the OT-ωB97X-D/6-31G** level of theory in blend.*

References

1   L. Kronik, T. Stein, S. Refaely-Abramson and R. Baer, *J. Chem. Theory Comput.*, 2012, **8**, 1515–1531.

2   T. Stein, L. Kronik and R. Baer, *J. Am. Chem. Soc.*, 2009, **131**, 2818–2820.

3   B. Yang, Y. Yi, C.-R. Zhang, S. G. Aziz, V. Coropceanu and J.-L. Brédas, *J. Phys. Chem. C*, 2014, **118**, 27648–27656.

4   T. Kastinen, M. Niskanen, C. Risko, O. Cramariuc and T. I. Hukka, *Phys. Chem. Chem. Phys.*, 2016, **18**, 27654–27670.

5   T. Kastinen, D. A. da Silva Filho, L. Paunonen, M. Linares, L. A. Ribeiro Junior, O. Cramariuc and T. I. Hukka, *Phys. Chem. Chem. Phys.*, 2019, **21**, 25606–25625.

6   T. Kastinen, M. Niskanen, C. Risko, O. Cramariuc and T. I. Hukka, *J. Phys. Chem. A*, 2016, **120**, 1051–1064.

7   J. Lu, S. Zhu, Z. Zhou, Q. Wu and G. Zhao, *Int. J. Quantum Chem.*, 2006, **106**, 2073–2081.

8   L. Benatto and M. Koehler, *J. Phys. Chem. C*, 2019, **123**, 6395–6406.

9   K. Do, M. K. Ravva, T. Wang and J.-L. Brédas, *Chem. Mater.*, 2017, **29**, 346–354.

10   J. L. Brédas, D. Beljonne, V. Coropceanu and J. Cornil, *Chem. Rev.*, 2004, **104**, 4971–5003.

11   V. Lemaur, M. Steel, D. Beljonne, J.-L. Brédas and J. Cornil, *J. Am. Chem. Soc.*, 2005, **127**, 6077–6086.

12   L. Cupellini, P. Wityk, B. Mennucci and J. Rak, *Phys. Chem. Chem. Phys.*, 2019, **21**, 4387–4393.

13   R. A. Marcus, *J. Chem. Phys.*, 1965, **43**, 679–701.

14   P. Song, Y. Li, F. Ma, T. Pullerits and M. Sun, *Chem. Rec.*, 2016, **16**, 734–753.

15   T. Liu and A. Troisi, *J. Phys. Chem. C*, 2011, **115**, 2406–2415.

16   L. Pandey, PhD Thesis, Georgia Institute of Technology, 2013.

17   U. C. Singh and P. A. Kollman, *J. Comput. Chem.*, 1984, **5**, 129–145.

18   B. H. Besler, K. M. Merz and P. A. Kollman, *J. Comput. Chem.*, 1990, **11**, 431–439.

19   C.-H. Yang and C.-P. Hsu, *J. Chem. Phys.*, 2013, **139**, 154104.

20   A. A. Voityuk and N. Rösch, *J. Chem. Phys.*, 2002, **117**, 5607–5616.

21   C.-P. Hsu, *Acc. Chem. Res.*, 2009, **42**, 509–518.

22   C. Wang, S. Ni, S. Braun, M. Fahlman and X. Liu, *J. Mater. Chem. C*, 2019, **7**, 879–886.

23   H. Meng, Y. Li, B. Pang, Y. Li, C. Zhan and J. Huang, *J. Mater. Chem. C*, 2019, **7**, 8442–8449.

24   W. Zhao, S. Li, H. Yao, S. Zhang, Y. Zhang, B. Yang and J. Hou, *J. Am. Chem. Soc.*, 2017, **139**, 7148–7151.

25   B. Gao, H. Yao, J. Hou, R. Yu, L. Hong, Y. Xu and J. Hou, *J. Mater. Chem. A*, 2018, **6**, 23644–23649.

26   Y. Wang, Y. Zhang, N. Qiu, H. Feng, H. Gao, B. Kan, Y. Ma, C. Li, X. Wan and Y. Chen, *Adv. Energy Mater.*, 2018, **8**, 1702870.

27   M. M. Szumilo, E. H. Gann, C. R. McNeill, V. Lemaur, Y. Oliver, L. Thomsen, Y. Vaynzof, M. Sommer and H. Sirringhaus, *Chem. Mater.*, 2014, **26**, 6796–6804.

28   S. Shi, J. Yuan, G. Ding, M. Ford, K. Lu, G. Shi, J. Sun, X. Ling, Y. Li and W. Ma, *Adv. Funct. Mater.*, 2016, **26**, 5669–5678.

29   L. Lan, Z. Chen, Q. Hu, L. Ying, R. Zhu, F. Liu, T. P. Russell, F. Huang and Y. Cao, *Adv. Sci.*, 2016, **3**, 1600032.

30   S. Li, L. Ye, W. Zhao, H. Yan, B. Yang, D. Liu, W. Li, H. Ade and J. Hou, *J. Am. Chem. Soc.*, 2018, **140**, 7159–7167.

31   W. Li, L. Ye, S. Li, H. Yao, H. Ade and J. Hou, *Adv. Mater.*, 2018, **30**, 1707170.

32   Z. Xu, Q. Fan, X. Meng, X. Guo, W. Su, W. Ma, M. Zhang and Y. Li, *Chem. Mater.*, 2017, **29**, 4811–4818.

33   B. Fan, L. Ying, P. Zhu, F. Pan, F. Liu, J. Chen, F. Huang and Y. Cao, *Adv. Mater.*, 2017, **29**, 1703906.

34   H. Zhang, H. Yao, J. Hou, J. Zhu, J. Zhang, W. Li, R. Yu, B. Gao, S. Zhang and J. Hou, *Adv. Mater.*, 2018, **30**, 1800613.

35   B. A. Abdulahi, X. Li, M. Mone, B. Kiros, Z. Genene, S. Qiao, R. Yang, E. Wang and W. Mammo, *J. Mater. Chem. A*, 2019, **7**, 19522–19530.

36   M. M. Durban, P. D. Kazarinoff and C. K. Luscombe, *Macromolecules*, 2010, **43**, 6348–6352.

37   Z. Zhang, W. Liu, T. Rehman, H.-X. Ju, J. Mai, X. Lu, M. Shi, J. Zhu, C.-Z. Li and H. Chen, *J. Mater. Chem. A*, 2017, **5**, 9649–9654.